2019 SECED Conference
Earthquake risk and engineering towards a resilient world
9-10 September 2019, Greenwich, London

MIXED PROBABILISTIC SEISMIC DEMAND MODELS FOR FRAGILITY ASSESSMENT

Akrivi CHATZIDAKI[1] & Dimitrios VAMVATSIKOS[2]

Abstract: *A mixture model is presented for combining the results of different models or analysis approaches into a single probabilistic seismic demand model that is suitable for fragility assessment. A structure can be represented using different model types or even levels of resolution for the same type, while it may also be analysed via methods of different complexity, most notably static versus dynamic nonlinear approaches. Combining the results from different models or analysis methods can be beneficial as it allows updating the results of a simpler approach or combining the strengths of two different models. For example, different model types may offer accuracy advantages in complementary response regions. This is the case of distributed-plasticity fiber models that offer higher fidelity for reinforced concrete frames at low (pre-capping) deformations, while lumped-plasticity models are more reliable for larger (post-capping) deformations closer to collapse. Through the combination of the results of both models we can potentially better capture the performance of the frame at all levels of seismic intensity. By employing a minimal 5 parameter power-law-based model we offer viable options for forming mixed probabilistic seismic demand models that can combine both different models and different analysis methods into a single output suitable for fragility assessment.*

Introduction

The Performance-Based Earthquake Engineering (PBEE) framework, originally developed by Cornell and Krawinkler (2000) for the Pacific Earthquake Engineering Research (PEER) Center, is commonly employed for seismic risk assessment. The PBEE methodology can be summarized as an implementation of the total probability theorem:

$$\lambda(DV) = \int_{DM}\int_{EDP}\int_{IM} G(DV \mid DM)\left|dG(DM \mid EDP)\right|\left|dG(EDP \mid IM)\right|\left|d\lambda(IM)\right| \quad (1)$$

where *IM* is the ground motion Intensity Measure (e.g. peak ground acceleration, spectral acceleration), *EDP* is the Engineering Demand Parameter (e.g. maximum interstory drift ratio), *DM* is the damage measure and *DV* is the Decision Variable. The final product of this calculation is the mean annual frequency of exceeding *DV*. Thus, risk can be estimated in terms of decision variables that make sense even to non-engineers such as casualties, monetary loss, repair cost, or down time.

Of essence in this calculation is the estimation of the third term of Eq. (1) which represents the fragility curve. System fragility curves arise naturally from the partitioning of the continuous *DM* to *N* discrete damage states, DS_i (i = 0...N-1), separated by N-1 associated limit-states LS_i, i = 1…N-1. Each fragility curve is a continuous function that provides the probability of exceeding a given LS_i, or equivalently of being in DS_i or worse, given the IM. They can be expressed as:

$$F_{LSi}(IM) = P\left[LS_i \text{ violated} \mid IM\right] = P\left[D > C_{LSi} \mid IM\right] \quad (2)$$

where limit state LS_i violation is typically defined as the seismic demand, D, exceeding the associated limit-state capacity, C_{LSi}. The most comprehensive analytical methods for fragility assessment rely on advanced numerical models subjected to nonlinear response history analyses (NLRHA). Single-stripe analysis (e.g. Jalayer and Cornell 2009), multistripe analysis (e.g. Jalayer 2003, Jalayer and Cornell 2009), cloud analysis (e.g. Jalayer 2003) or Incremental Dynamic Analysis (IDA, Vamvatsikos and Cornell 2002) can be performed to derive such curves (Bakalis and Vamvatsikos 2018).

[1] PhD candidate, National Technical University of Athens, Athens, cakrivi@central.ntua.gr
[2] Assistant Professor, National Technical University of Athens, Athens

However, different models of the same structure tend to offer different accuracy at complementary response regions. This is the case when lumped- or distributed-plasticity elements are employed to model a reinforced concrete (RC) structure. Distributed-plasticity models consist of fiber elements that allow representation of phenomena such as concrete cracking and gradual plastification of sections, thus they can better reproduce the behavior of the structure in the pre-yield segment. However, they fail to capture the post-capping response of the system and they often fail to converge in the region of negative global lateral stiffness. On the contrary, lumped-plasticity elements can model the post-capping response well enough but often fail to capture the transition of the system from the initial uncracked stiffness to the cracked one, thus they cannot reproduce well enough the pre-yield structural response. At the same time, they offer an easier convergence thus they can be applied when multiple NLRHA are performed even close to collapse. To overcome such model accuracy and convergence constraints, a mixed surrogate model can be employed and used for fragility assessment, able to combine the results of both lumped- and distributed-plasticity models, at the response region where each one in more reliable.

Case-study building

To illustrate the proposed framework, a 4-story RC building is studied. The building has two perimeter MRFs of four bays that act in each principal direction and internal columns that carry only gravity loads. The plan view of the building and the elevation of the moment frame are shown in Figure 1. The overall plan dimensions are about 55x37m (120'x180') while the total height is about 16.5m (54'), with a 4.5m (15') fist story and 4m (13') height of each of the remaining stories. Dead load of 8.4kN/m^2 (175psf) and live load of 2.4kN/m^2 (50psf) were assumed, with the latter not acting on the roof of the building. The building was designed by Aschheim et al. (2019) following a performance-based approach that enables the direct design of the structure subject to a set of predefined performance objectives through the use of the Yield Frequency Spectra (Vamvatsikos and Aschheim 2016). A single performance objective was targeted during the design to limit the MAF of exceeding an interstory drift ratio of 2% under dynamic response to 2.11x10^{-3}, which is equivalent to a 10% probability of exceedance in 50 years, while a confidence level against uncertainties of 68% was adopted.

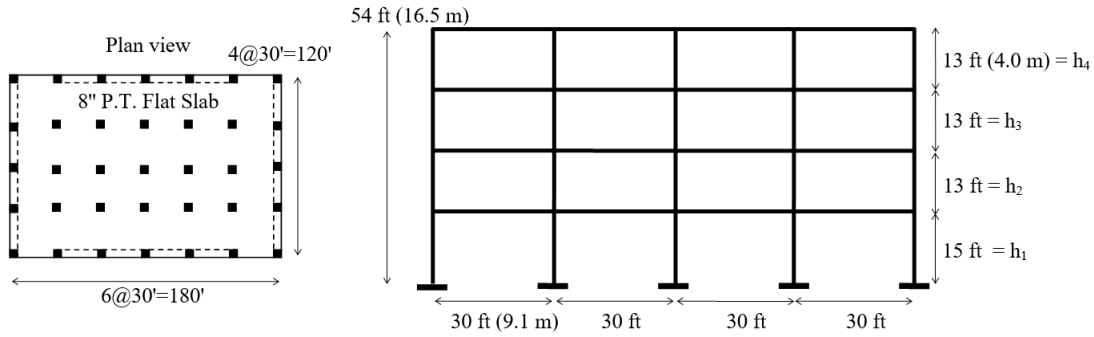

Figure 1. Plan view of the building and elevation of the perimeter moment resisting frame (adopted from Aschheim et al. 2019).

Modeling

A two-dimensional model of the building was prepared in OpenSees (Mazzoni et al. 2000). Only one out of the two perimeter 4-story and four-bay moment resisting frames that act in each principal direction was modeled along with a leaning column. The leaning column was pinned at the foundation and modeled using linear elastic elements having cross sectional properties of one half of the gravity columns of the building plus one half of the columns that belong to the moment frames acting in the other direction. The 2D model of a building may employ either lumped- or distributed-plasticity elements. Lumped-plasticity elements are computationally more efficient but are based on phenomenological models of the plastic-hinges that cannot capture axial-moment interaction or the spreading of inelasticity. On the contrary, distributed-plasticity fiber-element models can model the evolution of plasticity throughout both the member and the section while accounting for axial force and bending moment interaction at a considerable higher computational cost. On the other hand, the simpler lumped plasticity models are far more robust, especially in

the negative stiffness region of response, and can thus better capture collapse. Herein, both modes were employed.

In the distributed-plasticity model, beams and columns were modeled using force-based fiber elements discretized into longitudinal steel and concrete fibers. A bilinear constitutive law accounting for pinching and stiffness degradation was used to model the steel reinforcing bars. The unconfined cover concrete was modeled without confinement, while the confinement related parameters of the core concrete were calculated on the basis of the Mander et al. (1988) model. The strength of the steel and concrete materials was set at their expected values, rather at nominal characteristic strengths, thus f_{ye} = 475MPa (69ksi) and f_{ce} = 44.8MPa (6.5ksi). To simulate the rigid diaphragm, frame nodes were rigidly connected by stiff truss elements at each floor level. One end of each horizontal beam element was provided with a low stiffness axial spring at the connection with the column. This solution was preferred instead of imposing rigid kinematic constraints. Such constraints would impose the condition of zero axial strain on beams resulting in the generation of fictitious axial compression forces increasing the bending moment capacity of beam sections. Rayleigh damping of 1% was assigned to the first and second mode. Although this is lower than a typical value of 5% usually assigned to reinforced concrete structures, it is considered realistic as cracking is directly incorporated in the fiber model giving rise to early hysteretic damping.

In the lumped-plasticity model, beams and columns were modeled using a single force-based beam-column element per member with plastic hinges located at each end. Moment-rotation laws for each plastic hinge were defined in terms of the backbone curve of ASCE SEI 41/13. As suggested in ASCE SEI 41/13 instead of the sudden drop at the post-capping region of the moment-rotation law, a more gradual slope was implemented. Rigid kinematic constrains were applied on all nodes of each floor thus enforcing the same lateral displacements. Regarding the stiffness properties of the interior elastic part of each member, typically the code suggests that the effective stiffness EI of the elements should be reduced to account for cracking of the member. As mentioned in ASCE-SEI 41/13, if I_g is the gross section moment of inertia and E is Young's modulus for concrete, one should employ $0.3EI_g$ for non-prestressed concrete beams and 0.3 or $0.5EI_g$ for concrete columns, depending on the design axial load acting on each member. Although this approach stems from analyses targeting a conservative result, it is common practice to extend it to cases were unbiased results should be sought, such as in performance-based design, introducing considerable inaccuracies. For this reason, two different lumped-plasticity models were created, namely a *non-calibrated* and a *calibrated*. In the non-calibrated model, the aforementioned EI_g values were adopted while in the calibrated case the "cracked" moment of inertia of both beams and columns was increased by averaging the initial "uncracked" stiffness and the nominal "cracked" stiffness at yield, as derived by moment-rotation analyses of the actual fiber sections. This calibration allowed for better matching the pre-yield behavior of the lumped- and the distributed-plasticity models, thus reducing the differences in response for low-to-moderate levels of deformation.

A Rayleigh damping of 5% was assigned in the first and second mode for the lumped-plasticity models. In all cases, P-Δ effects were accounted for via a first-order treatment.

Analysis results

The static pushover capacity curves resulting from a first-mode-proportional lateral load pattern are shown in Figure 2 for all models in terms of base shear and maximum interstory drift ratio, θ_{max}. The fundamental period of the distributed-plasticity model, the calibrated and the non-calibrated lumped-plasticity models are $T_{1,f}$ = 0.82sec, $T_{1,cl}$ = 0.99sec and $T_{1,ncl}$ = 1.71sec, respectively. Note that the small difference in the fundamental periods of the calibrated lumped and the distributed-plasticity model is not of concern as it is only indicative of the higher stiffness in the fully uncracked model that only exists for small deformations. The true effect of the calibration of the lumped-plasticity model is obvious in the match of the pre-yield segments of the calibrated lumped and the distributed-plasticity model. The non-calibrated model, by being far more flexible, fails to capture the pre-yield segment of the response of the fiber model, and will thus be discounted henceforth.

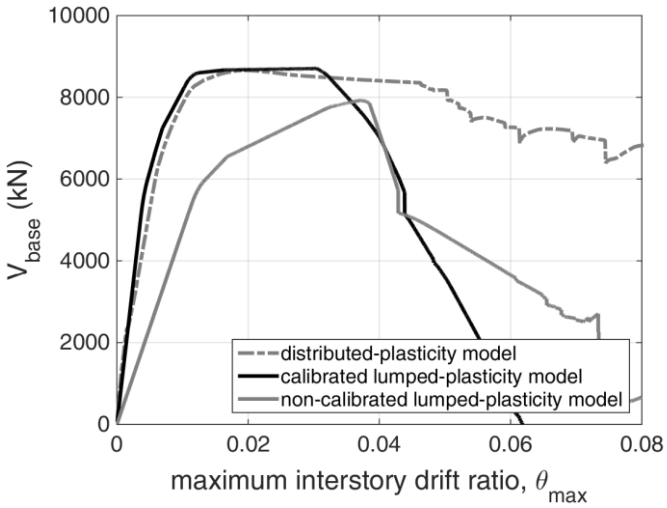

Figure 2. Static pushover capacity curves of the distributed-plasticity model (grey dash-dotted line) versus the calibrated (black line) and non-calibrated (grey solid line) lumped-plasticity ones.

IDA was performed in all models using the far-field ground motion set of FEMA P695 (FEMA 2009). This set comprises of 22 ground motions, each having two horizontal components, resulting in a total of 44 accelerograms. The first-mode spectral acceleration at the fundamental period of each structure was adopted herein as the IM, thus $Sa(T_{1,cl},5\%)$ and $Sa(T_{1,f},5\%)$ were used for the calibrated lumped- and the distributed-plasticity model, respectively. The maximum interstory drift over all stories at each time step, θ_{max}, was chosen as the EDP. Individual record IDA curves along with their 16%, 50% and 84% fractiles are presented for illustrative purposes in Figures 3 a-b for the fiber and the calibrated lumped-plasticity model. IDA 16, 50 and 84% fractiles are shown in Figure 3c for both models after being modified to the same IM, i.e. the spectral acceleration at the fundamental period of the calibrated lumped-plasticity model.

In Figure 3 we can observe that the variability in structural response for low IMs is higher for the distributed-plasticity than the lumped-plasticity model. Structural variability can be directly estimated through IDA quantiles since the greater the distance between the 16% and 84% quantiles is, the higher the variability. This comes as no surprise since distributed-plasticity models do exhibit variability up to the nominal yield due to the contribution of higher modes and because they are already manifesting some non-linear response, as cracking appears and plasticity is developed. On the contrary, in lumped-plasticity models an assumption of initial elastic behavior has been made thus the variability in the response for low IMs is only influenced by the higher modes. This lower variability of the lumped-plasticity model at low IM levels may potentially bias the results especially when low-damage limit states are being examined (e.g. damage limitation).

For higher IMs the opposite tendency seems to appear. Due to convergence issues, the distributed-plasticity model even for relatively low IMs seems to have collapsed and flatlines in IDA curves are artificially generated. Therefore, EDP-IM points with high EDP values do not appear in the results resulting in a lower variability in the structural response for higher IMs. On the contrary, lumped-plasticity models converge easier even at high IMs so they can retain such EDP-IM pairs resulting in higher variability. The lower variability of the distributed-plasticity model in this region cannot be consider representative of the actual behavior of the system as it is caused due to the inability of the system to converge.

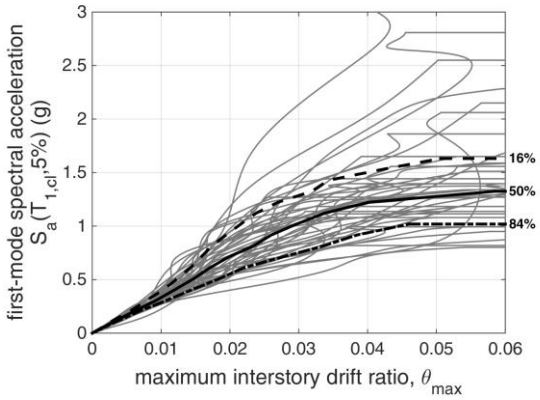

(a) calibrated lumped-plasticity model

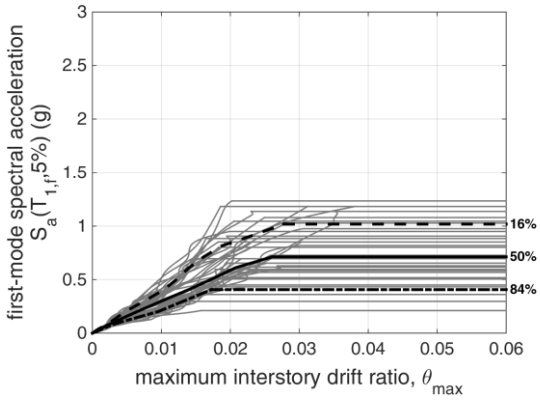

(b) distributed-plasticity model

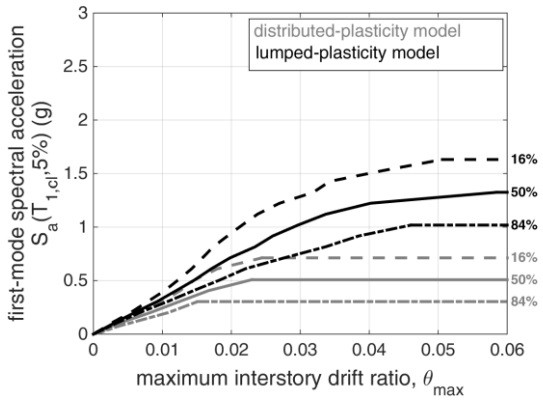

(c) IDA fractiles modified to the same IM

Figure 3. Incremental Dynamic Analysis results for the (a) calibrated lumped-plasticity model and (b) the distributed-plasticity model in terms of the first-mode spectral acceleration of each model and maximum interstory drift ratio, θ_{max}. The 16%, 50% and 84% IDA fractiles of both models are shown in (c), after being modified to the spectral acceleration at the fundamental period of the calibrated lumped-plasticity model.

Fragility assessment via mixed modeling

The aforementioned observations generate thoughts on the suitability of either single model for fragility assessment, and the potential for improvement by combining their respective results. To give preference to each model where we know its predictive power to be higher, one option is to assign relative weights to their results. This is essentially a Bayesian belief that one model is more reliable than the other, thus a higher weight (or probability) can be assigned to the former and a lower to the latter. For low IMs, the fiber model seems to better capture the structural response distribution, thus a higher weight should be assigned. For higher IMs, the lumped-plasticity model is considered to be much more reliable and this should be translated into the weight assigned. The selection of the relative weights will depend on the details of the case at hand but obviously by modifying the relative weights we can vary the mixed model results to capture either of the two models and any combination in between.

An interesting question of computational significance is how many nonlinear analyses to employ for estimating the response of each model. At one end, full IDA can be performed for both models, as in Figure 3, and their results combined in postprocessing. Given our previous observations for the case at hand, results of the distributed-plasticity model for *Sa* < 0.3g were combined with those of the lumped-plasticity model for *Sa* > 0.3g and the empirical fragility curves of Figures 5 a-c were derived for θ_{max} = 1.0, 1.5 and 3.0%, respectively. These limit states were indicatively selected to cover the range of structural response up to the point where the fiber model can contribute to the results. The empirical fragility curves were estimated as the fraction of analyses exceeding *LS* capacity for each *IM* level. An obvious non-monotonicity is observed in fragility curves near the critical *Sa* of 0.3g since up to this value fiber model results are used for the

generation of the fragility curve and from this value and above, those of the lumped-plasticity model were used. Interpolation, discarding the higher of the two IMs for each probability level or some more complex fitting approach may be employed to restore the desired monotonicity.

Obviously, employing full IDAs is an expensive solution that (at least for the case at hand) also requires some post-processing to achieve monotonic results. Instead, only a few, say 4, stripes can be performed and the results can be more easily combined via weighted regression to estimate fragility. The lumped-plasticity model can better reproduce the behavior of the structure for higher IM levels and near collapse thus two stripes can be performed with this model. In the fiber model, two stripes of analyses should be performed for relatively low IM levels aiming to capture the variability in the structural response at this region. The results of the two models can be combined for fragility assessment by assigning relative weights to each one and applying a five-parameter power-law based approximation (Jalayer and Cornell 2009) that comprises of a linear regression in the log-log space for the no collapse data and a logistic regression for collapse data.

In cases where sparse data is available, as is the case at hand since only a limited number of stripe analyses are performed, a form of regression needs to be applied in order to obtain a continuous EDP|IM representation. Generally, the model chosen for the regression does influence the results yet simpler models are preferable for our purposes. Cornell et al. (2002) proposed the power-law approximation of Eq. (3):

$$EDP = a \cdot IM^{b} \varepsilon \tag{3}$$

where b is the slope in log-space, ln(a) is the intercept and ε is the lognormal random variable with unit median and a logarithmic standard deviation of $\sigma_{ln\varepsilon}$. The basic assumption of this approach is that the EDP|IM dispersion is constant for all IM levels hence by globally applying Eq. (3) a constant dispersion for all IMs is assumed. The linear fit in the log-log space of Eq. (3) provides reasonable results when data in the no collapse region are processed. Global collapse is generally deemed to occur when numerical non-convergence appears in a rigorous model that incorporates both material and geometric nonlinearities and large values of EDP are captured. Such large or infinite EDP values would bias the results at lower IMs if a single regression was to be applied in all data. To overcome this issue, collapsing points were treated separately via logistic regression to estimate probability of collapse given the IM. It can be expressed as:

$$\ln\left(\frac{P[C \mid IM]}{1-P[C \mid IM]}\right) = b_0 + b_1 IM \tag{4}$$

where $P[C \mid IM]$ is the probability of collapse given the IM and b_0, b_1 are parameters estimated trough the regression. Other alternatives for the estimation of $P[C \mid IM]$ do exist, such as the method of moments or the maximum likelihood method (Baker 2015).

The total probability theorem can be applied for a given level of *IM* to combine the results of the mutually exclusive events of Collapse, *C*, and No Collapse, *NC*. The probability of exceeding a *LS* for a given level of *IM* is defined as:

$$P[EDP > EDP_C \mid IM] = P[EDP > EDP_C \mid NC, IM](1-P[C \mid IM]) + 1 \cdot P[C \mid IM] \tag{5}$$

where $P[EDP > EDP_C \mid C, IM]$ always equals 1.0. The resulting $P[EDP > EDP_C \mid IM]$ is a mixture distribution that depends on the individual distributions of *C* and *NC* and a lognormal curve may not fit the computed fragility curve. For a given limit state, the terms of Eq. (5) are estimated according to Eq. (3) and (4). Consequently, a fragility curve for a given limit state can be directly determined if a total of five parameters are estimated; three for the no collapse points (i.e. a, b and $\sigma_{ln\varepsilon}$) and two for collapse data (i.e. b_0 and b_1). It should be noted that adding more terms in the linear regression for the *NC* points may result in a more flexible model but at the same time it may overfit the data. In general, when limited analysis data is available, the five-parameter model is preferred for simplicity.

In the case at hand, two stripes were performed with the distributed-plasticity model at $Sa(T_{1,cl})$ = 0.1g and 0.15g and two for the lumped-plasticity model at $Sa(T_{1,cl})$ = 0.85g and 1.2g. For each stripe 20 NLRHA were conducted using records from the far-filed ground motion set of FEMA P695. The two higher stripes were employed for collapse fragility assessment. The results indicate that more than 16% of the records caused structural collapse in the higher second stripe of the lumped-plasticity model. For this reason, this stripe was excluded from the power-law fitting

of the no collapse data. Consequently, to estimate the probability of demand exceeding capacity given no collapse, $P[EDP > EDP_c \mid NC,IM]$, only the lower three stripes were employed.

The lower three stripes employed in fitting Eq. (3) appear in Figure 4. Different assumptions regarding the relative weights of the two models were made and the power-law approximation of Eq. (3) was applied to estimate the P[EDP > EDP_C |*NC,IM*]. The resulting linear fits are also presented for two extreme cases having $w_l = 0.00 – w_f = 1.00$ (dash-dotted grey line) and $w_l = 1.00 – w_f = 0.00$ (dash-dotted black line), as well as for $w_l = 0.10 – w_f = 0.90$ (grey solid line), where w_l and w_f are the relative weights assigned to the lumped and the distributed plasticity model, respectively. In the case of w_l=1.00, given that only one stripe of results is available and the slope of the linear fit in the log-log space cannot be computed analytically, a value of 1.0 was adopted for the latter.

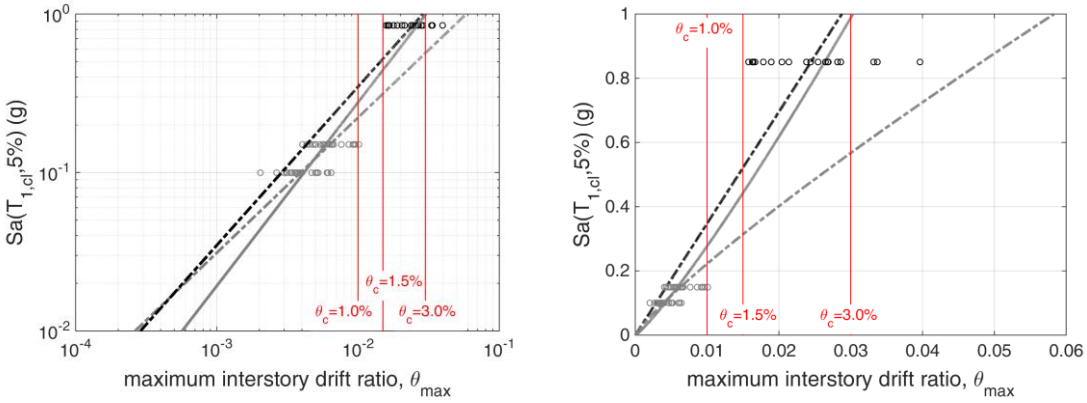

(a) log-log coordinates (b) linear coordinates

Figure 4. IM-EDP stripes considered in the power-law fit of the lumped-plasticity (back color) and the distributed-plasticity model (grey color). The power-law based approximation is shown for $w_f = 1.00 – w_l = 0.00$ (dash-dotted grey line), $w_f = 0.00 – w_l = 1.00$ (dash-dotted black line) and $w_f = 0.90 – w_l = 0.10$ (grey solid line). For the latter case, the slope of the linear fit in the log-log space was assumed to be equal to 1.00. The red lines indicate the θ_C values of three limit states that were examined.

In Figures 5 a-c the fragility curves for different combinations of the relative weights of the lumped- and the distributed-plasticity model are presented for θ_C = 1.0%, 1.50% and 3.0%. The empirical fragility curves calculated based on IDA results along with those computed by applying Eq. (5) for each single model are also presented for comparison purposes. It is worth mentioning that the weights assigned in the two models are not indicative of their relative importance, since they highly depend on the leverage of the lumped-plasticity model's stripe performed at a higher IM level than the two stripes of the distributed-plasticity model. However, the results can be regularized to obtain the relative importance of the two models for each case. Obviously, by modifying the relative weights of the lumped- and the distributed-plasticity models, the fragility curves of the mixed model can capture the response of either of the two models and any combination in between.

For comparison purposes, the mean annual frequency (MAF) of exceeding each limit state, for the fragility curves of Figure 5 was also computed. The MAF of exceeding a limit state can be estimated considering the last two terms of Eq. (1) as:

$$\lambda(D > C) = \int P\left(D > C \mid IM\right)\left|d\lambda\left(IM\right)\right| \tag{6}$$

where $|d\lambda(IM)|$ is the differential of the hazard curve and $P(D > C \mid IM)$ is the fragility curve of a given limit state. The hazard curve of San Jose California (latitude = 37.33659° and longitude = 121.89056°) was used to estimate MAFs and the results for all limit states are listed in Table 1. The empirical fragility curves estimated trough IDA results (Figure 5 black solid lines) were converted to monotonic ones simply by ignoring the vertical dropdown of the curve and adopting the lowest IM point wherever multiple such points are provided at any given probability level.

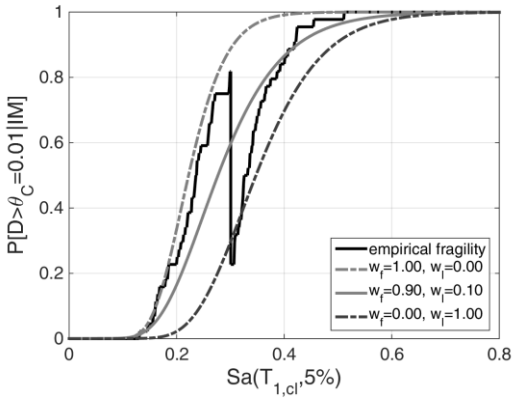

(a) θ_C = 1.0%

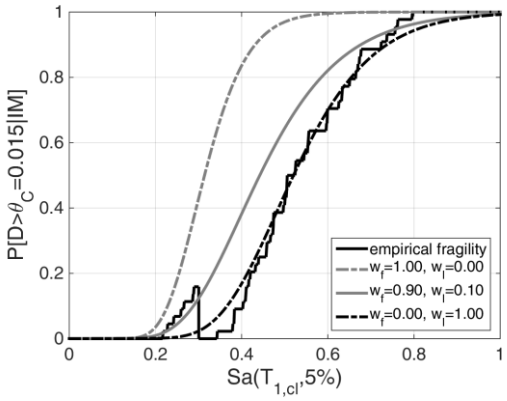

(b) θ_C = 1.5%

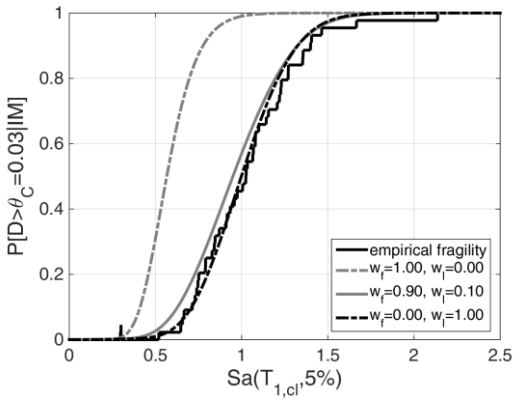

(c) θ_C = 3.0%

Figure 5. Empirical fragility curves from IDA results of the fiber model for Sa < 0.3g and lumped-plasticity model for Sa > 0.3g (black solid line) and fragility curves estimated through the mixed model when different weights were applied on each model. The weights highly depend on the leverage of the stripes and do not represent the relative importance of each model. Three limit states are examined i.e. (*a*) θ_C *= 1.0%,* (*b*) θ_C *= 1.5% and* (*c*) θ_C *= 3.0%.*

weights	**θ_c = 1.0%**	**θ_c = 1.5%**	**θ_c = 3.0%**
w_f = 1.00 – w_l = 0.00	0.0233	0.0135	0.0041
w_f = 0.90 – w_l = 0.10	0.0174	0.0076	0.0013
w_f = 0.00 – w_l = 1.00	0.0114	0.0050	0.0010
monotonically made empirical fragility	0.0205	0.0060	0.0010

Table 1. Mean annual frequency of exceeding LS for different fragility curves.

For θ_c = 1.0%, when w_f = 100% the obtained fragility curve matched well enough with the portion of the empirical fragility coming from IDA results of the fiber model. The θ_c value for this limit state is close to the stripe results of the fiber model, as can be observed in Figure 4, which allows an accurate estimation of the fragility. On the contrary, when w_l = 100% the derived fragility curve could not reproduce the empirical one of lumped-plasticity model's IDA results. This was expected to happen, since the targeted LS was far from the regions where results of the lumped-plasticity model were available (see Figure 4). The fragility curve derived from the fiber model is more conservative than the one of the mixed model thus resulting in a higher MAF. This is attributed to the small difference in low Sa values, which by the way, are the most critical ones when it comes to MAF estimation. By employing the mixed model with w_f = 0.90 and w_l = 0.10 the derived fragility curve offers a good compromise between the two models.

For θ_c = 1.5% the opposite tendency seems to appear regarding matching the portion of the empirical fragility curve with the computed fragilities through the five-parameter power law based approximation for each single model. This limit state, falls in a region far from the stripe results

where not enough data is available. For instance, in Figure 4 neither of the three stripes crosses the θ_c = 1.50% vertical line. For this reason, for 100% weight assigned on the fiber model, the obtained fragility curves fails to perfectly capture the one estimated through IDA results. For 100% weight on the lumped plasticity model, the fragility curve seems to well reproduce the behavior of IDA results but this is generally not the rule in regions where not enough data is available. By employing the mixed probabilistic model, the obtained fragility curve is a combination of those of the two models. In terms of MAF, although the fiber-model offers more conservative results (i.e. higher MAF) it cannot be considered representative of the actual performance of the system in this θ_c region. The mixed model may offer more reliable results, yet only comparison with a true benchmark could offer solid evidence in favor of one or the other.

For θ_c = 3.0% the fragility curve of the fiber model seems not to be able to capture the performance of the system. In this region, the distributed-plasticity model cannot be considered reliable since stripe results are far from the LS being examined. However, the lumped plasticity model seems to better reproduce the behavior of the building and even if a relatively high weight is assigned to the fiber model, the results fall closer to those of the lumped plasticity model. The MAF of exceeding this LS when only the lumped-plasticity model is used is about the same as the one obtained through the (forced to become monotonically) empirical fragility. Generally, given the stripe analysis results (as per Figure 4) one may directly understand whether each model should be treated separately or how the two models should be combined into a mixed model.

Conclusions

The presented approach can take into account different analysis options into a single output suitable for fragility assessment by using a weighted combination of different sets of results. In this case, the example shown by the five-parameter power-law-based model, originally introduced by Jalayer (2003), enabled us to obtain reliable estimations of the fragility curves even in regions where not enough data was available. The selection of the relative weights assigned to each model depends on user's own preferences and beliefs about the validity of each model in each region. Obviously, by modifying the relative weights, the mixed probabilistic seismic demand model is capable of capturing the response of each single model and any combination in between.

Acknowledgements

Financial support has been provided by the Eugenides Foundation in Greece and by the Innovation and Networks Executive Agency (INEA) under the powers delegated by the European Commission through the Horizon 2020 program "PANOPTIS-development of a decision support system for increasing the resilience of transportation infrastructure based on combined use of terrestrial and airborne sensors and advanced modelling tools", Grant Agreement number 769129.

References

ASCE 41-13: Seismic Evaluation and Retrofit Rehabilitation of Existing Buildings. In: *Proceedings, SEAOC 2012 Convention*, 2012.

Aschheim M, Hernández-Montes E and Vamvatsikos D (2019), Design of Reinforced Concrete Buildings for Seismic performance: Practical, deterministic and probabilistic approaches, CRC Press

Bakalis K and Vamvatsikos D (2018), Seismic Fragility Functions via Nonlinear Response History Analysis, *Journal of Structural Engineering*, 144(10): 1–15

Baker JW (2015), Efficient Analytical Fragility Function Fitting Using Dynamic Structural Analysis, *Earthquake* Spectra, 31(1): 579–599

Cornell CA and Krawinkler H (2000), Progress and Challenges in Seismic Performance Assessment, PEER Center News 2000, 3(2): 1–4

Cornell CA, Jalayer F, Hamburger RO and Foutch D (2002), Probabilistic Basis for 2000 SAC 737 Federal Emergency Management Agency Steel Moment Frame Guidelines, *Journal of Structural Engineering*, 184(4): 526-533

FEMA (2009). FEMA P695 Far field ground motion set. Available at: http://users.ntua.gr/divamva/resourcesRCbook/FEMA-P695-FFset.zip (Accessed 27/01/2019)

Jalayer F (2003), *Direct probabilistic seismic analysis: Implementing nonlinear dynamic assessments*, Ph.D. Thesis, Dept. of Civil and Environmental Engineering, Stanford: Stanford University

Jalayer F and Cornell CA (2009), Alternative non-linear demand estimation methods for probability-based seismic assessments, *Earthquake Engineering & Structural Dynamics*, 38(8): 951–972

Mander BJ, Priestley JM and Park R (1988), Theoretical stress-strain model for confined concrete, *Journal of Structural Engineering*, 114(8): 1804–1826

Mazzoni S, McKenna F, Scott M and Fenves G (2000), Open system for earthquake engineering simulation: OpenSees command language manual, University of California, Berkeley, CA. (Accessed online http://opensees.berkeley.edu, January 2019)

Vamvatsikos D, Aschheim M (2016), Performance-based seismic design via yield frequency spectra, *Earthquake Engineering and Structural Dynamics*, 45(11):1759–1778

Vamvatsikos D and Cornell CA (2002), Incremental dynamic analysis, *Earthquake Engineering & Structural Dynamics*, *31*(3): 491-514